

HILBERT HUANG TRANSFORM FOR WIRE DIAGNOSTICS IN AIRCRAFT

Mokhtar Sadok⁽¹⁾, Norden E. Huang⁽²⁾, and Michael Walz⁽³⁾

(1) Mokhtar Sadok is a senior scientist at Goodrich Corporation

(2) Norden E. Huang is a senior fellow at NASA Goddard Space Flight Center

(3) Michael Walz is the manager of the FAA Aging Aircraft Electrical Systems Program

Abstract

This study discusses the feasibility of using Time-Frequency Domain Reflectometry (TFDR) for Wire Diagnostics based on the Hilbert Huang Transform (HHT). The studied approach is developed to detect and locate “hard” defects (i.e. opens and shorts) as well as “soft” (i.e. intermediary impedance) defects in all types of wires, including the challenging case of single wires. Another outcome of the study is determining the optimal bandwidth for Time Domain Reflectometry (TDR) devices.

The proposed approach has been applied to a database of wire signatures collected using a fast TDR of 35 Pico second rise-time and 20 GHZ bandwidth. This research effort is funded by the FAA and is undertaken by Goodrich in response to a Broad Agency Announcement (BAA) to advance the Development of Electrical Wiring Interconnect System Test and Inspection Systems.

1. Background

Wire diagnostics is essential to further the goal of aircraft safety, readiness, and profitability. Historically, aircraft wiring was assumed to last the life of the aircraft. This has prompted the FAA to publish new proposed rules and guidance on wire maintenance and inspection. These guidelines are published under the Enhanced Airworthiness Program for Airplane Systems/Fuel Tank Safety (EAPAS/FTS). Under this NPRM the FAA “are proposing new maintenance, inspection and design criteria for airplane wiring to address conditions that put transport airplanes at risk of wire failures, smoke, and fire.”[1] To comply with this proposed rule new technology needs to be developed to nonintrusively inspect the condition of installed wire on aircraft. . After investigating several technologies, Time Domain Reflectometry (TDR) is found to be a practical technology for wire diagnostics at this time.. One of the advantages of TDR is that it requires connection to only one end of the wire, overcoming the access problems associated with double-ended measurements. The technique is based on injecting a fast rising DC step pulse into the wire under test then monitoring and evaluating the resulting reflections. A perfectly matched line will generate no reflections, while a mismatched line, either due to defects or interconnects, will provide a reflection informative of the impedance profile of the wire under test. Although traditional use of TDR proved useful in identifying hard defects such as opens and shorts in controlled impedance environments, it is less effective at locating soft faults, or even opens and shorts, in non-impedance controlled environments such as the case of single wires.

Single wires are, by far, the most challenging case for TDR-based diagnosis mainly because of the associated uncontrolled impedance environment. Distance between the wire under test and its return path affects directly the measured impedance when operating at high frequency. Unlike the case of coaxial cables or twisted pair where the return path is controlled to a great extent, the distance between the wire and its return path in the case of single wires is not typically constant given the anticipated bending and movement of wires. A specific study to quantify the effect of distance variation on the TDR-based diagnosis of single wires has been submitted for publication elsewhere [2].

2. Hilbert Huang Transform

The Hilbert Huang Transform (HHT) is a time-frequency analysis technique designed to deal efficiently with nonlinear and nonstationary data [3-4]. The key-part of the HHT method consists of decomposing intricate data into a finite and small number of intrinsic mode functions (IMFs) that reflect local properties of the signal and admit well-behaved Hilbert transform. The process of decomposing raw data into a finite set of IMFs is called Empirical Mode Decomposition (EMD). The Hilbert transformation of those IMFs provides an energy-frequency-time distribution giving sharp and meaningful identifications of imbedded features. Unlike typical spectral analysis approaches, where the basis functions are fixed and pre-determined a priori, the EMD method adaptively decomposes the signal into oscillating components extracted from the data itself.

2.1. The Empirical Mode decomposition (EMD)

The premise of the EMD technique is to project the data in a basis of oscillatory modes called Intrinsic Mode Functions (IMF) extracted from the data itself. Because the approach is algorithmic, it does not allow an analytic expression of the different components of the EMD in a closed form. There are two conditions for a given function to be considered as an IMF:

- i) The function has the same numbers of zero crossings and extrema
- ii) The function has symmetric envelopes defined by the local maxima and minima respectively. In other words, the extrema must be symmetric with respect to the local mean of the function.

The first condition, similar to the sine wave requirement, is put to ensure sharp frequency localization. The second condition is necessary to ensure that spectral analysis will not cause undesired frequency artifacts induced by asymmetric waveforms. The EMD algorithm iteratively sifts through data to generate IMF functions varying from high to low frequency. The algorithm converges if the actual IMF has only two extrema (e.g. a monotonic function) or less (e.g. a constant function). In such case, the IMF is the residue of the decomposition; it represents the DC part or the trend of the original signal. If N is the total number of the Intrinsic Mode Functions then, after convergence of the algorithm, the original signal can be written as:

$$x(t) = \sum_{i=1}^N IMF_i(t) + r_N(t) \quad (1),$$

where $r_N(t)$ is the decomposition residue after sifting up to the N^{th} IMF. The sifting process of the EMD algorithm is akin to the process of dilation and translation in the wavelet transform. The first set of IMFs carry the high frequency content of the signal whereas the last ones carry the low frequency content of the signal.

2.2. Hilbert Transform

Hilbert transform is a well known technique for extraction of instantaneous frequency and energy components from highly nonstationary and nonlinear data [5]. The Hilbert transform, $Y(t)$, of an arbitrary time series, $X(t)$, is given by:

$$Y(t) = \frac{1}{\pi} P \int_{-\infty}^{+\infty} \frac{X(\alpha)}{(t - \alpha)} d\alpha \quad (2)$$

Where P is a normalizing constant. Equation (2) defines the Hilbert transform as a convolution product of the original signal $X(t)$ with $f(t)=1/t$ that emphasizes local properties. Define the complex signal $Z(t)$ as:

$$Z(t) = X(t) + iY(t) = A(t)e^{i\theta(t)} \quad (3)$$

Hence,

$$\begin{cases} A(t) = \sqrt{X^2(t) + Y^2(t)} \\ \theta(t) = \arctan\left(\frac{Y(t)}{X(t)}\right) \end{cases} \quad (4)$$

The polar representation of the original signal $X(t)$, as given by Equation 4, indicates that such a representation is the best local fit to $X(t)$. The instantaneous frequency is given by:

$$f(t) = 2\pi \frac{d\theta(t)}{dt} \quad (5)$$

Let the instantaneous frequency of the i^{th} IMF be

$$f_i(t) = 2\pi \frac{d\theta_i(t)}{dt} \quad (6)$$

where $\theta_i(t)$ represents the instantaneous phase of the i^{th} IMF. At a given instant t , there will be a vector of amplitudes $A(t)$ corresponding to different frequencies of the IMFs (i.e. $A(f,t)$). The final result, known as the Huang-Hilbert Transform (HHT), is a time-frequency-energy distribution representing the instantaneous Hilbert spectrum energy:

$$S_H(f, t) = 20 \log(A^2(f, t)) \quad (7)$$

3. Application to Single Wire Diagnostics

A wire harnesses consisting of a 10-foot bundle of several wire types (i.e. single, twisted pair, shielded twisted pair, triple twisted pair, and coaxial) is used in this study. Small damages are inflicted on those wires and TDR reflections were collected to test the HHT proposed approach. Figure 2 shows an example of the inflicted damage on a twisted pair of the studied wire bundle. All damages are located around the middle of the 10-foot harness within a few inches. Damages are in the order of 1 to 2 cm abrasions applied to the exterior shield. In the single wire case, about 1-cm of the wire plastic coat covering the conductor is stripped off.

The 20 GHz bandwidth TDR (i.e. Tektronix CSA8200) is used to assess the feasibility of detecting small abrasions in single wires. Single wires are in fact the most challenging case for a TDR-based approach since the return path is not controlled as mentioned previously. Figure 3 shows a typical CSA8200 measurement of the 10-foot single wire reflection with a 0.75 inch-abrasion around the distance 4.6 feet. The single wire, subject of this study, is connected to pin 11 of the harness while another single wire connected to pin 13 of the harness is taken as a return path since it is physically the closest to pin 11. Eight different signatures, similar to the one shown in Figure 3, have been collected for this study. At every measurement the harness is moved and twisted to simulate installation and environmental variability.

Starting with the Empirical Mode Decomposition, each signature is decomposed into its Intrinsic Mode Functions (IMFs) to be subsequently processed by the Hilbert Transform. Figure 4 shows the 10 IMFs generated by the EMD process for the single wire-based TDR signature of Figure 3. Notice that each IMF has symmetric envelopes with respect to the time line and has the same number of extrema and zero crossings as required by the definition of an IMF.

The first set of IMFs (i.e. 1 to 5) is mainly high frequency noise and carries no information of interest. The last set of IMFs (i.e. 8 to 10) is low frequency information unrelated to the defect dynamics. The sixth IMF and, to a lesser extent, the seventh IMF are the most informative modes for detection. Figure 5 shows the sixth IMF (the most informative mode) of all eight TDR samples plotted together.

In some cases, where wire defects are noticeable, the IMF information could be used as a solid indication for detection. In some other cases, the IMF information may provide a useful hint for defect detection. However, in this challenging case, it is not obvious to make such a conclusion based only on the IMF information.

Instantaneous frequency information, shown in Figure 6, provides a better basis for detection. Typically at the defect spot, instantaneous frequency jumps indicating the presence of nonstationarity and most likely the presence of an anomaly. Two major observations can be pointed out by looking at Figure 6. First, there is an unexpected rise of the instantaneous frequency around the 2-foot distance that is not due to a wire defect, per say. Such a rise is in fact due to the tight fastening of the wire bundle around 2-foot distance. The second observation is that after the defect spot around 4.6 feet, the instantaneous frequency response started to exhibit a high degree of variability and fluctuations around the mean which could be captured in some way to enhance defect detection. However, such variability makes it also harder to put together a simple threshold-based strategy for detection.

Figure 7 shows instantaneous frequencies generated using the IMFs number 6 and 7 bearing most information about the defect. In particular, instantaneous frequency of the sixth IMF captures clearly the defect effect around 4.6 feet. It was found in many cases that instantaneous frequency of the sixth IMF is sufficient enough to make a decision about the defect presence and location. However, in some other cases, such indicator by itself was not quite decisive.

To provide more consistent time-frequency characterization, the Hilbert transform is applied to the set of IMF bearing the high frequency content of the signal under test. Figure 8 shows the Hilbert spectrum of the first seven IMF functions and a zoom of the spectrum around the frequency band [0 2] GHz where most of the signal energy is concentrated. Although the Hilbert spectrum of this particular signal is not quite decisive, the mean Hilbert spectrum of all measurements, shown in Figure 9, is more informative. The two major events, including the inflicted abrasion, are sticking out on the HHT-based time-frequency representation. The spectrum shows that most of the very high frequency above 1 GHz is basically noise with no information of interest.

Small defects on other types of wires, including coaxial and twisted pair, and “hard defects”, such as opens and shorts, are not included in this study because of their relative ease compared to the problem at hand.

4. TDR Bandwidth

One of the goals of this study is to determine an optimal TDR bandwidth for wire diagnostics. As they are typically unshielded and because of the associated uncontrolled return path, single wires represent a worst case study for high bandwidth TDR.

Figure 10 shows the marginal signal energy versus frequency of the first 7 IMF functions of the single wire-related TDR reflection of Figure 3. The energy distribution of such a typical reflection shows that most of the signal energy is located in the frequency band under 1 GHz. This is an interesting finding as it shows that going higher in frequency won't buy much after an upper limit in the neighborhood of 1 GHz is reached. Figure 6 that shows the instantaneous frequency profile of several single wire signatures validates this result further. Most of the energy in the frequency band above 1 GHz undergoes a 20 dB loss or more making it in the order of noise level. Thus, it is recommended to use a TDR of at least 1-GHz bandwidth for wire diagnostics.

5. Conclusion

Application of Time-Frequency techniques has shown promise for wire diagnostics. The Hilbert Huang Transform (HHT) was used to provide Time-Frequency representations out of TDR signatures. The HHT-based time-frequency approach was tested over a set of single wires signatures

collected via a fast TDR of 35 Pico second rise-time and 20 GHZ bandwidth. Another finding of this study was the determination of a lower bandwidth limit for TDR-based wire diagnostics.

6. References

- [1] Federal Register/Vol. 70, No. 193 58509 October 6, 2005 “Enhanced Airworthiness Program for Airplanes Systems / Fuel Tank Safety (EAPAS/FTS); Proposed Advisory Circulars; Proposed Rule and Notices , Executive Summary p.3
- [2] Sadok, M, Amara Boujemaa, R., and Jaidane, M, “A proof of non Robustness of Reference-based TDR Methods for Diagnosis in Single Wires” to appear on the 14th European Signal Processing Conference (EUSIPCO), September 4-8, 2006, Florence, Italy.
- [3] Huang, N. E., et al. “The empirical mode decomposition and the Hilbert spectrum for nonlinear and nonstationary time series analysis”, Proceedings of the Royal Society London. A, 454, pp. 903-995, 1998.
- [4] Huang, N. E. “A new Method for Nonlinear and Nonstationary Time Series Analysis: Empirical Mode Decomposition and Hilbert Spectral Analysis” Proceedings of the SPIE, Orlando FL, April 2000, pp. 197-209.
- [5] Bendat, J and Piersol, A, “Random Data Analysis and Measurement Procedures”, John Wiley & Sons, Inc. Third Edition, NY 2000.
- [6] Cohen, L, “Time Frequency Distributions – A review”, Proc. IEEE, Vol 77, n°7, 1989.

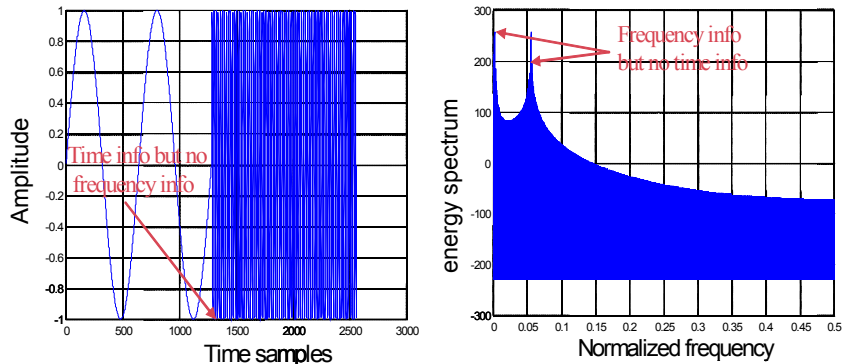


Figure 1a. Original signal: a frequency switch (left) and its Fourier-based Power Spectral Density (right). When moving from one domain to another either frequency or time domain information is lost.

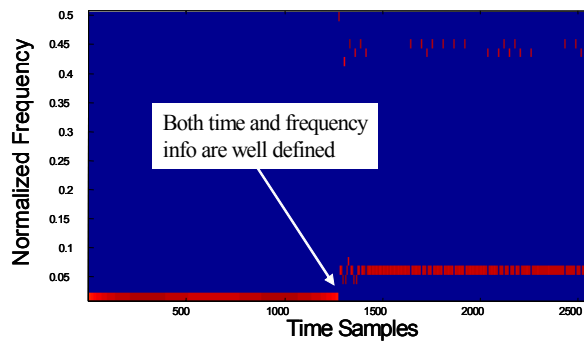


Figure 1b. Energy spectrum in a Time-Frequency Representation (TFR) of the above signal computed using the Hilbert Huang Transform. Both time (i.e. 500) and frequency (i.e. 0.01 and 0.05) are well defined.

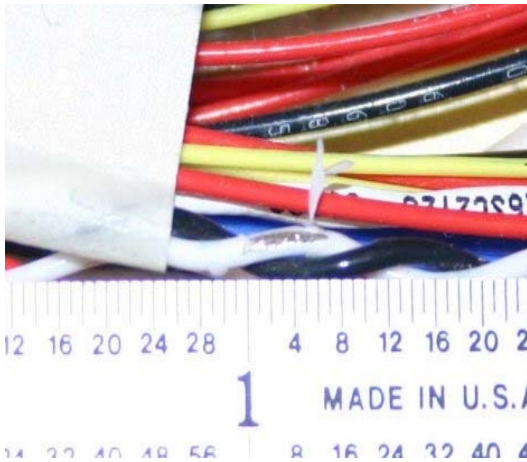


Figure 2. Example of a typical defect inflicted on the 10-foot wire bundle

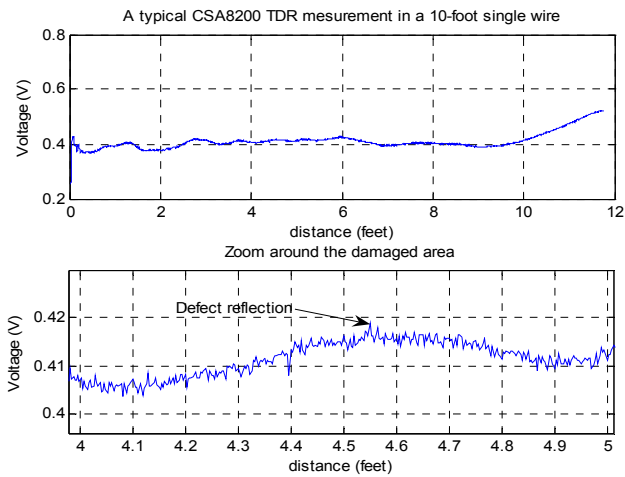


Figure 3. A typical CSA8200 TDR measurement in a 10-foot single wire within a bundle.

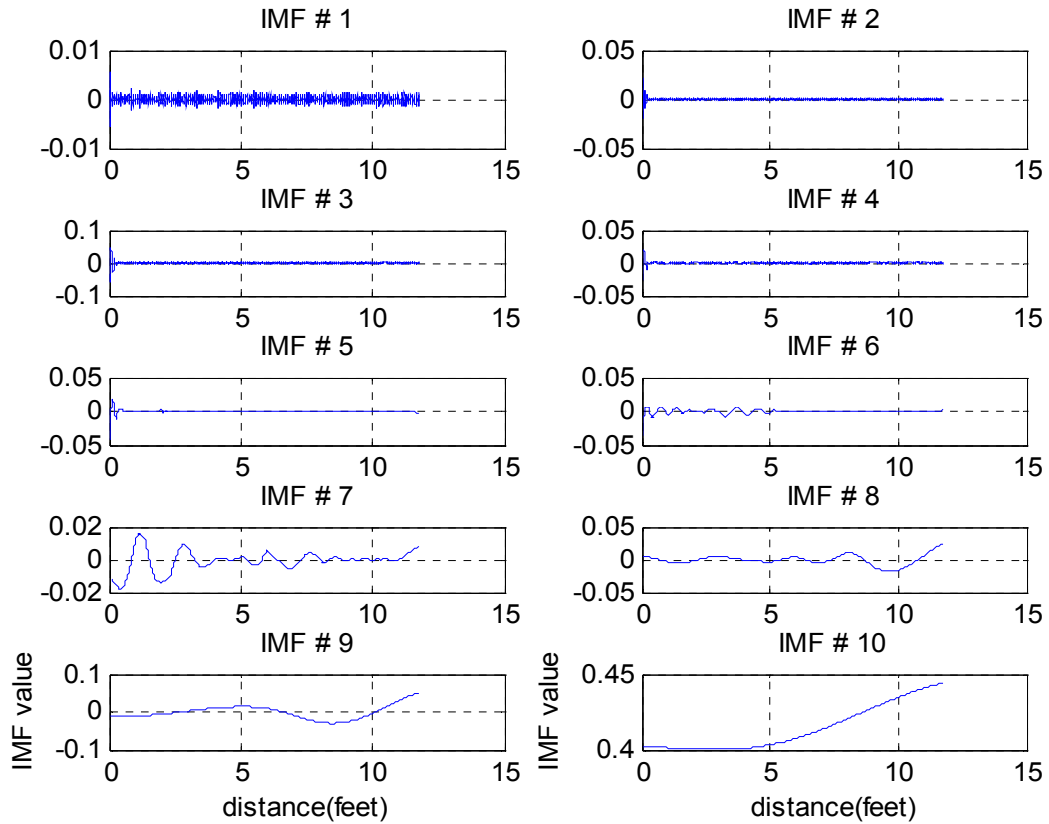


Figure 4. Example of Empirical Mode Decomposition of a CSA8200 TDR signature for a 10-foot single wire.

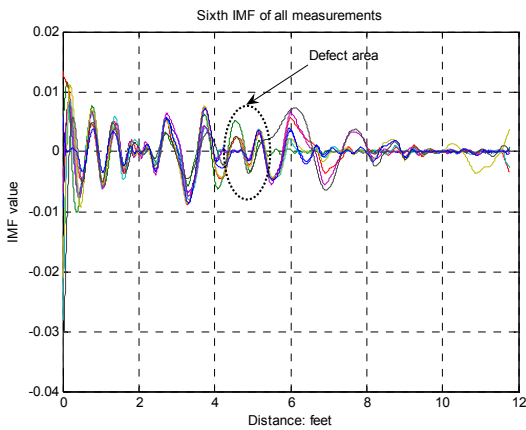


Figure 5. The sixth IMF of all TDR samples

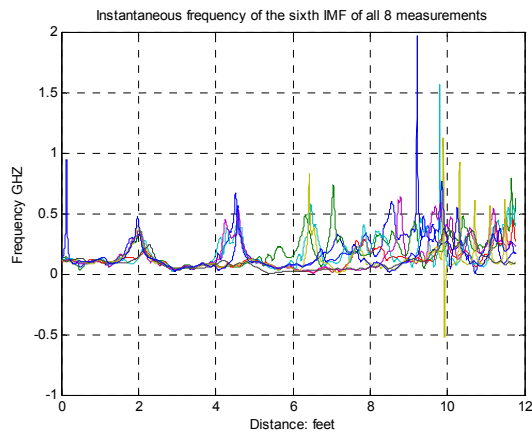


Figure 6. Instantaneous frequency variation of the sixth IMF of the eight TDR samples.

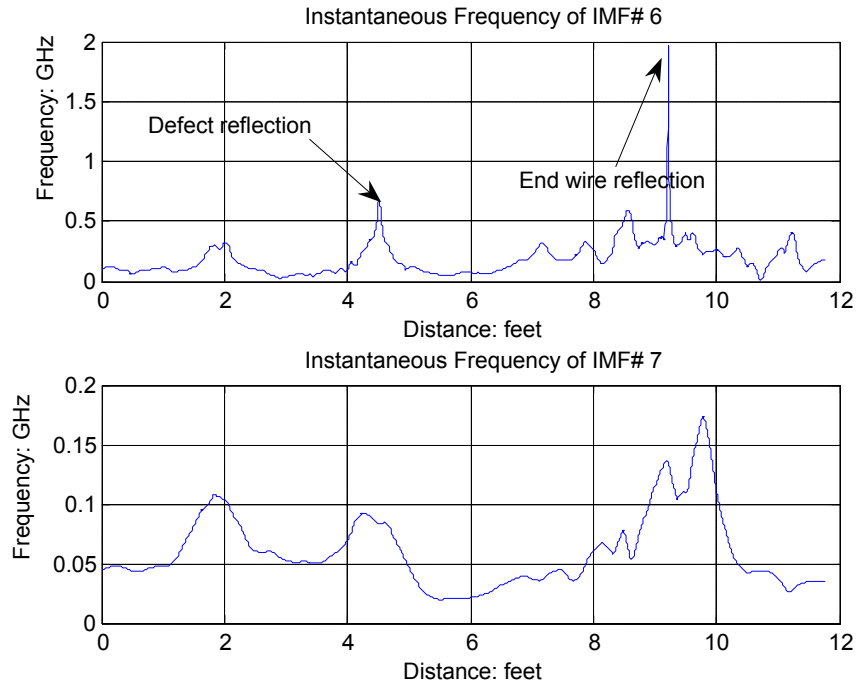


Figure 7. Instantaneous frequency representation of IMFs 6 and 7 of the previous example. Note that most of the information of interest is located under 1 GHz.

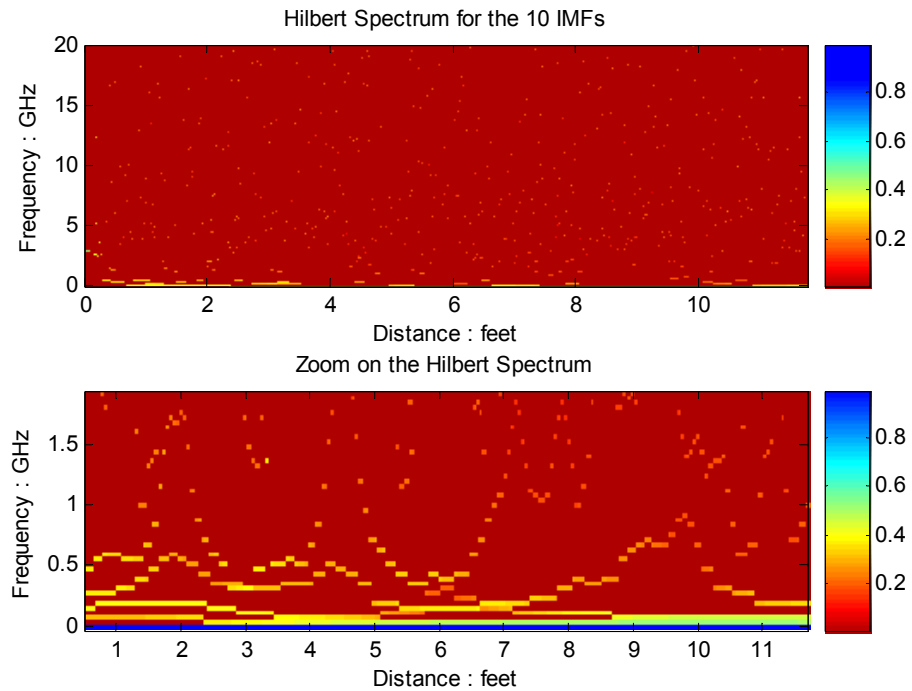


Figure 8. Hilbert spectrum of all IMFs of the signal shown at Figure 4 with a zoom in the [0 2] GHz band.

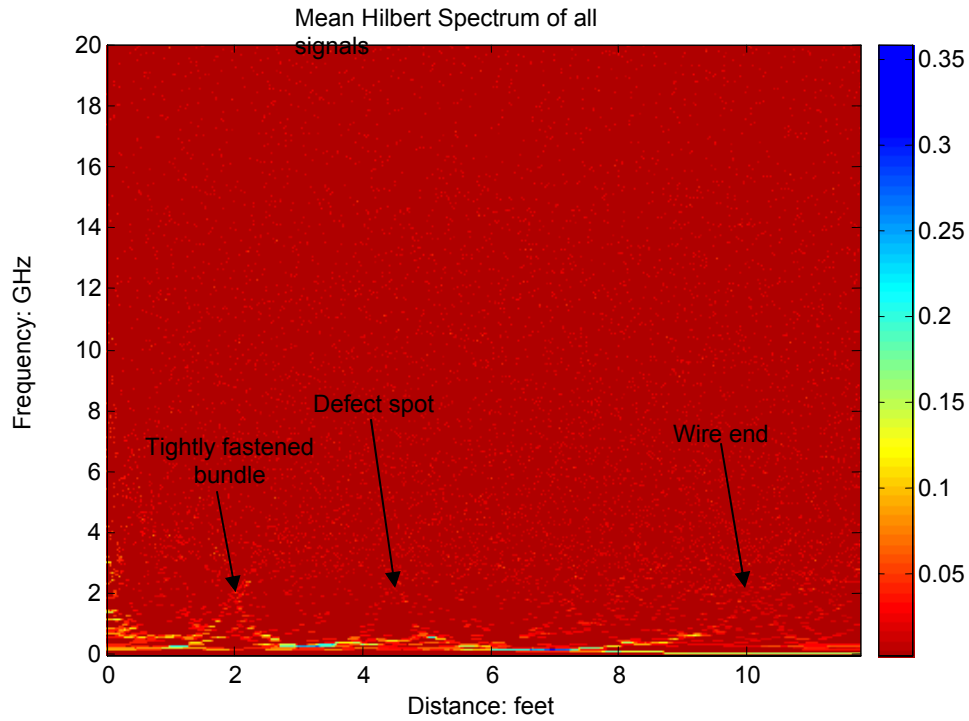


Figure 9. Joint time-frequency representation of the mean Hilbert spectrum of all signatures.

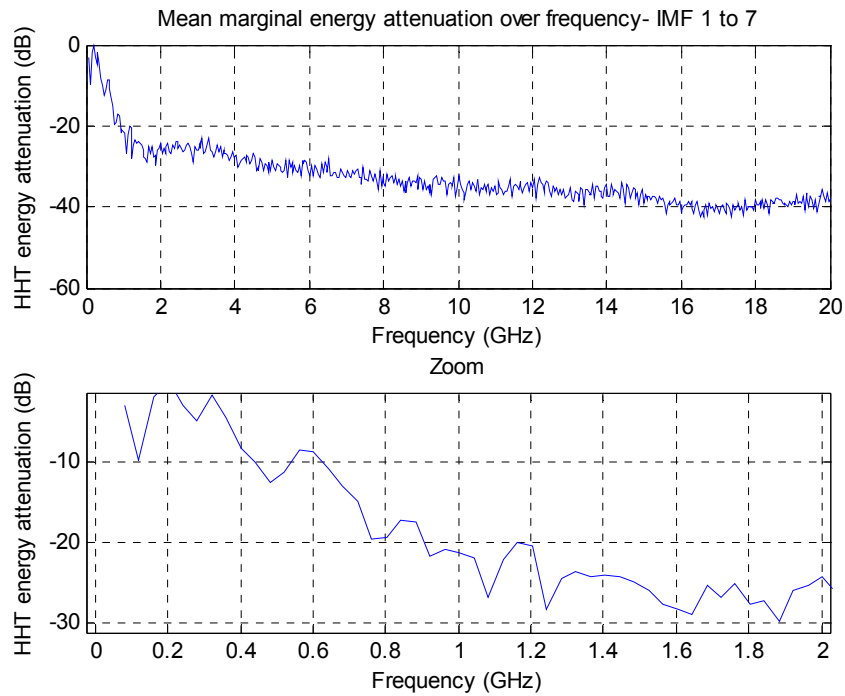


Figure 10. Mean marginal frequency distribution of all signals considering IMF1 to IMF7